On the Factors Affecting Battery Unit Contributions to Fault Currents in Grid-Connected Battery Storage Systems

Saleh A. Saleh , *Senior Member, IEEE*, Emre Ozkop , *Senior Member, IEEE*, Marcelo E. Valdes , *Fellow, IEEE*, Ahmet Yuksel , *Student Member, IEEE*, Mohammed Haj-Ahmed , *Member, IEEE*, Zaid G. Sanchez, *Member, IEEE*, and Claudio S. Mardegan , *Senior Member, IEEE*

Abstract—This article investigates factors affecting the contributions of battery units to fault currents in grid-connected battery storage systems (BSSs). The work in this article is intended to examine the effects of the state-of-charge (SOC) on battery currents that are drawn due to faults. This article also examines the impacts of charger controller actions on the currents drawn from battery units to faults in grid-connected BSSs. The impacts of the SOC and charger controller on battery currents due to faults are examined for the lead-acid, lithium-ion, and nickel–cadmium battery units. Examination results show that the battery currents due to faults are directly dependent on the SOC. Moreover, these results show that actions of charger controller can support the battery terminal voltage, thus preventing the fast reduction of the SOC. The support of the battery terminal voltage helps in limiting the currents drawn from battery units during faults. The effects of the SOC and charger controller are verified using a 1-MW, 3ϕ grid-connected BSS, which has lead-acid battery units. Several faults have been created during charging and discharging operations, and at different values of SOC. Test results confirm the direct dependence of battery currents (due to faults) on the SOC. In addition, obtained results demonstrate the ability of charger controller to limit the currents drawn from battery units due to faults in different parts of a grid-connected BSS.

Index Terms—Grid-connected battery storage systems, grid-connected power electronic converters, IEEE Standard 946, IEEE Standard 1375, power system faults.

I. INTRODUCTION

A. General

HIGH-POWER-RATED battery storage systems (BSSs) have gained popularity in power systems due to their fast response, high power density, and dynamic charge/discharge characteristics. Applications of BSSs in power systems include supporting voltage/frequency stability, improving the power quality, and mitigating variations of the power generated by renewable energy systems [1]–[9]. Despite their capabilities to enhance power systems functions, the interconnection of BSSs can create challenges for protection systems and devices. Such challenges are created by [1]–[8]

1) bidirectional power flows to charge/discharge the BSS;
2) actions of the BSS controller to regulate the power flow;
3) features of interfacing power electronic converters (PECs); and
4) contributions of the BSS to fault currents.

References [10]–[13] provide various aspects for designing accurate and reliable protection systems for interconnected BSSs. Test results of these protection systems have demonstrated their abilities to accommodate bidirectional power flows, actions of BSS controllers, and features of interfacing PECs [1], [13]. However, the accurate determination of BSS contributions to fault currents has not been fully addressed, when considering the actions of BSS controller and features of the interfacing PEC. In this regard, PECs used in interconnected BSSs are typically featured with built-in protection measures to limit the maximum current flowing through their switching elements. Furthermore, actions of the PEC controller are initiated to maintain the voltage on its ac side as close as possible to that of the host grid. Such controller actions represent additional limitations to the maximum current to flow through PEC switching elements during fault and nonfault events. These operational behaviors

Saleh A. Saleh is with the Department of Electrical and Computer Engineering, University of New Brunswick, Fredericton, NB E3B 5A3, Canada (e-mail: asaleh@unb.ca).

Emre Ozkop is with the Department of Electrical and Electronics Engineering, Karadeniz Technical University (KTU), 61080 Trabzon, Turkey (e-mail: eozkop@ktu.edu.tr).

Marcelo E. Valdes is with the ABB Electrical Solutions, Chapel Hill, NC 27517 USA (e-mail: marcelo.e.valdes@ieee.org).

Ahmet Yuksel is with the Energy Institute Ankara Branch, TUBITAK MAM, METU Campus, 41470 Gebze, Turkey (e-mail: ahmet.yuksel@tubitak.gov.tr).

Mohammed Haj-Ahmed is with the Department of Electrical Engineering, The University of Jordan, Amman 11942, Jordan (e-mail: m.hajahmed@ju.edu.jo).

Zaid G. Sanchez is with the Energy and Environment Center, Carlos Rafael Rodriguez University of Cienfuegos, Cienfuegos 59430, Cuba (e-mail: zgarcia@ucf.edu.cu).

Claudio S. Mardegan is with the EngePower, Santana de Parnaiba, Sao Paulo 06540-030, Brazil (e-mail: claudio.mardegan@engepower.com).
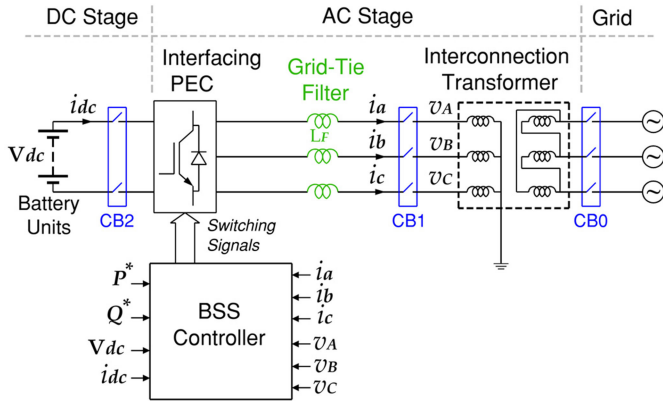
Fig. 1.   A circuit diagram for a 3ϕ grid-connected BSS.

of PECs and its controller (used in interconnected BSSs) directly impact the contributions of an interconnected BSS to fault currents.

B. Overview of IEEE Standard 946 and IEEE Standard 1375

BSSs have become essential components in many industrial systems, including data centers, communications systems, renewable energy systems, uninterrupted power supplies, power systems, and others. In these applications, a BSS is considered to have a dc stage and an ac stage that are fed from the utility grid via an interconnection transformer, as shown in Fig. 1. The dc stage is composed of the battery units and protection devices. The ac stage is composed of the interfacing PEC, grid-tie filter, interconnection transformer, grid-synchronizing, and protective devices [1], [3]–[6]. Several industrial sectors have developed standards and best practices for the design, operation, and protection for grid-connected BSSs [1]–[9].

Similar to other components of a power system, grid-connected BSSs can experience various types of faults, which can occur in the dc stage, ac stage, and grid. However, due to the charging and discharging operation of battery units, the behavior of a grid-connected BSS during faults can be influenced by several factors. For example, a fault in the dc stage during the charging operation may trigger a different current from the same fault, when it occurs during the discharging operation. An other example can be a fault in the ac stage may trigger a discharge current that is dependent on the state-of-charge (SOC) of the battery units [1]–[7], [13], [14]. In order to avoid equipment damages and/or service interruptions, grid-connected BSSs have to be featured with adequate protective devices (relays, circuit breakers, and fuses) with proper sizing and settings [1]–[5]. The selection of such protective devices requires determining currents that are triggered by faults at different stages of a grid-connected BSS.

IEEE Standard 1375

This standard [5] details recommended practices for the protection of stationary battery units. These battery units are typically connected to a dc bus that may feed some dc loads, and be connected to several PECs (chargers and inverters). The IEEE Standard 1375 addresses the short-circuit in battery units,

grounding of battery units, and protection devices for battery units. For faults in the dc stage, the IEEE Standard 1375 sets the battery contribution to the fault current based on

1) the battery time-constant;
2) the equivalent impedance as seen from the fault location; and
3) the battery-rated terminal voltage.

IEEE Standard 946

This standard [3] provides recommendations for designing stationary BSSs with a dc bus, dc loads, and multiple PECs (chargers and inverters). The IEEE Standard 946 provides guidance for designing protection systems for stationary BSSs, where protective devices are selected for ac and dc stages based on the maximum possible current triggered by faults in the ac and dc stages. This standard states that the maximum possible fault current is the sum of contributions by the battery units, active dc loads (connected to the dc bus), and filters on both sides of the charging PECs. The IEEE Standard 946 sets the contributions of battery units to faults in the ac or dc stages based on their rated voltages and equivalent impedance as seen from the fault location [1], [3], [10]–[14].

Other reported research works [15], [16] have investigated the protection of BSSs with different structures. In these works, the selection of the protective devices has been based on the IEEE Standards 1375 and 946. Moreover, the fault detection has been adapted from methods used in PEC protection as discussed [13], [17], [18]. Nonetheless, these works have not addressed the battery units contributions to fault currents.

C. Article Objectives and Contributions

Currents triggered by faults in grid-connected BSS have components contributed by the battery units and charger PEC. The existing methods to estimate these contributions do not consider the effects of the SOC and actions of the charger PEC. This article aims to investigate the factors affecting the currents drawn from battery units due to faults in grid-connected BSSs. The objectives of this article can be summarized as follows.

1) To examine effects of the controller actions on the currents drawn from battery units due to faults.
2) To examine the effects of the SOC on the battery currents during faults in a grid-connected BSS.

Achieving these objectives ensures the following contributions.

1) The factors (SOC and actions of BSS controller) affecting the currents drawn from battery units due to faults in grid-connected BSSs.
2) The verification of these factors using a 1-MW grid-connected BSS.

II. Fault Currents in Battery Storage Systems

There exist several approaches to determine fault currents in BSSs. Among these approaches are the IEEE Standard 1375 and IEEE Standard 946, which are intended for stationary BSSs. Fig. 2 depicts the single-line diagram for a stationary BSS.

The IEEE Standards 1375 and 946 determine a fault current, in a stationary BSSs, as a combination of contributions by
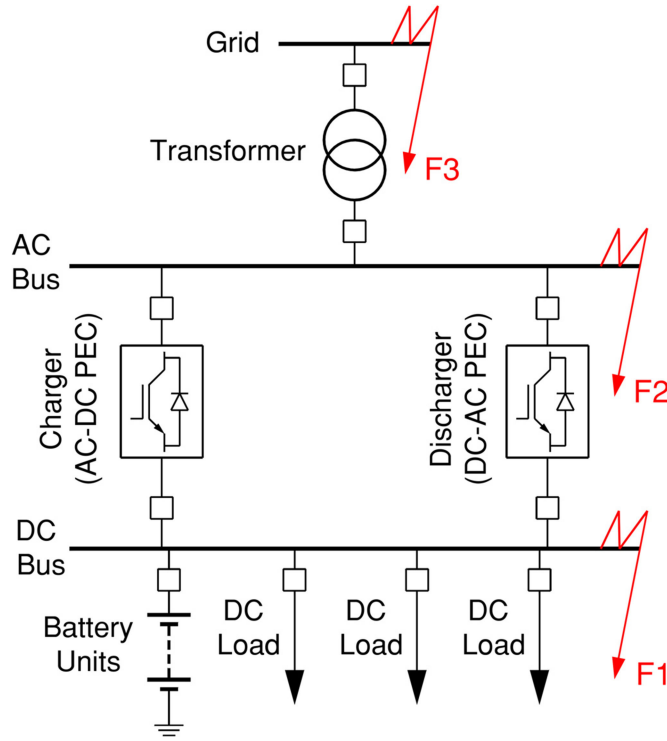
Fig. 2. A single-line diagram of a stationary battery storage systems [1].

the battery units and interfacing PECs (chargers and/or inverters) [1]–[6].

A. Calculating Fault Currents Using IEEE Standard 1375

The IEEE Standard 1375 sets the maximum current triggered by a fault in the dc bus (fault F1 in Fig. 2) as [5]

$$(i_{F1})_{\max} = \frac{V}{R}\left(1 - e^{-\frac{t}{\tau_{bs}}}\right) + 10\,(I_{\text{PEC}})_{\text{Rated}} \qquad (1)$$

where $(i_{F1})_{\max}$ is the maximum fault current triggered by F1, V is the prefault voltage on the terminals of the battery units, R is the equivalent resistance of the battery units, τ_{bs} is battery short-circuit time constant (see Table II in Ref. [5]), and $(I_{\text{PEC}})_{\text{Rated}}$ is the rated current of the charger. The IEEE Standard 1375 provides guidance for determining the value of R using the discharge characteristic curve of the battery units.

Remarks Regarding (1)
1) The value of $(i_{F1})_{\max}$ is intended only for determining the size and interruption capacity of protective devices to be installed in the dc bus.
2) The current contributed by the battery units to F1 is assumed to increase during the interval of $5 \times \tau_{bs}$ after the start F1. Nonetheless, this interval can be long enough for a significant reduction V, thus limiting the current contributed by the battery units.
3) The current contributed by the charger cannot exceed the rated pulsing current of individual switching elements comprising the charger. Such a current is less than $10(I_{\text{PEC}})_{\text{Rated}}$.

B. Calculating Fault Currents Using IEEE Standard 946

This standard determines the maximum current triggered by a fault in the dc bus (F1) as

$$(i_{F1})_{\max} = \frac{V_{Br}}{R_{eq}} + 10\,(I_{\text{PEC}})_{\text{Rated}} \qquad (2)$$

where V_{Br} is the rated terminal voltage of the battery units, and R_{eq} is the equivalent resistance seen in the location of F1. For a fault in the ac bus (Fault F2 in Fig. 2), the IEEE Standard 946 sets the maximum fault current as [3]

$$(i_{F2})_{\max} = 10\,(I_{\text{PEC}})_{\text{Rated}} + (i_{acI})_{\max}\left(1 + e^{-\gamma}\right) \qquad (3)$$

where $(i_{acI})_{\max}$ is the maximum ac current provided by the inverters (see Tables II and III in Ref. [19]), and γ is given as

$$\gamma = \frac{2\pi}{X/R}\left(0.49 - 0.1e^{-\frac{X/R}{3}}\right) \qquad (4)$$

with X being the equivalent inductive impedance seen from the location of F2, and R being the equivalent resistance seen from the location of F2.

For a fault on the grid side (fault F3 in Fig. 2), the contributions of the battery units and inverter, $(i_4)_{F3}$, are set by the IEEE Standard 946 as

$$(i_4)_{F3} = 10\,(I_{\text{PEC}})_{\text{Rated}}. \qquad (5)$$

The grid contribution to faults on the grid-side is determined using the IEEE Standard 3002.3 as [19]

$$(i_0)_{F3} = (i_{acG})_{\max}\left(1 + e^{-\gamma}\right) \qquad (6)$$

where $(i_{acG})_{\max}$ is the peak ac component of the grid current (see Tables II and III in Ref. [17]), and γ is determined by (4) for F3. The maximum current that can be triggered by F3, $(i_{F3})_{\max}$, is stated as

$$(i_{F3})_{\max} = 10\,(I_{\text{PEC}})_{\text{Rated}} + (i_{acG})_{\max}\left(1 + e^{-\gamma}\right). \qquad (7)$$

Remarks Regarding (3) and (7)
1) The values of $(i_{F2})_{\max}$ and $(i_{F3})_{\max}$, determined using the IEEE Standard 946, are used only for selecting the size and interruption capacity of protective devices in the dc and ac buses.
2) The contributions of battery units and inverter to faults in ac bus or grid are limited by the rated current of the inverter.
3) The contribution of the grid to fault currents in the ac stage can be determined using the IEEE Standard 3002.3.

III. FACTORS AFFECTING FAULT CURRENTS IN GRID-CONNECTED BSSs

In general, a battery unit can deliver an extremely high current during a short-circuit on its terminals. The short-circuit current delivered by a battery unit can reach more than 40 times its rated discharge current [1]–[4], [13]–[16]. However, short-circuit currents delivered by a battery unit can be affected by the battery type, SOC, protection devices, temperature, and equivalent resistance as seen from the terminals of the battery unit [18].
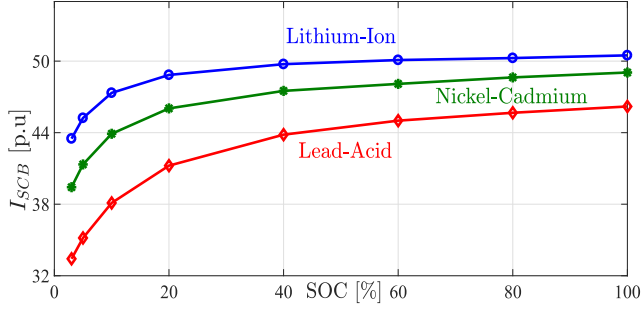
Fig. 3. Maximum short-circuit current at different values of the SOC for lithium-ion, nickel–cadmium, and lead-acid battery units. The base value of I_{SCB} is 8 A, and the value of Δt is $\Delta t = 10$ ms.
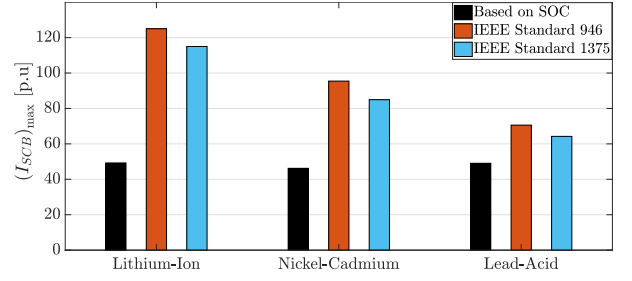

Fig. 4. Maximum short-circuit current for the tested lithium-ion, nickel–cadmium, and lead-acid battery units determined based on SOC= 100%, and IEEE Standards 946 and 1375. The base value of I_{SCB} is 8 A.

A. Effects of the SOC on the Short-Circuit Current

The SOC for a battery unit is a critical parameter that reflects its performance and facilitates its operation. The monitoring of the SOC of a battery unit helps preventing its overdischarge and improving its functions. The impacts of the SOC on the short-circuit of a battery unit can be illustrated by the relationship between the discharge current (I_{DS}) and SOC, that is [20]

$$I_{\text{DS}}(t) = \frac{C}{\Delta t} \left(\text{SOC}(t) - \text{SOC}\left(t - t_n\right) \right) \quad (8)$$

where C is nominal capacity of the battery unit in (Ah), Δt is a time interval, and t_n is set as $t_n = t - \Delta t$.

For purposes of demonstrating the effects of the SOC on the short-circuit current delivered by a battery unit, models for lithium-ion (LI-I), nickel–cadmium (N-C), and lead-acid (L-A) battery units have been created using e-TAP and MATLAB/SIMULINK software packages [21], [22]. These models have been used to test the short-circuit I_{SC} of these battery units at different values of the SOC. Each model is rated for 24 V, 20 A h, and a rated discharge current of 8 A. Fig. 3 shows the maximum short-circuit current at different values of the SOC for each battery unit.

Fig. 3 shows that the SOC value can have a significant influence on the maximum short-circuit current contributed by a battery unit. In addition, Fig. 3 demonstrates that the type of a battery unit has a direct influence on the maximum short-circuit current contributed by that battery unit.

The influences of the SOC on $(I_{SC})_{\max}$ are further demonstrated by a comparison with $(I_{SC})_{\max}$ determined by the IEEE Standards 946 and 1375 for three battery units. The internal resistances and short-circuit time constant for the LI-I, N-C, and L-A battery units are obtained from the data in Refs. [3] and [5] as follows.
1) LI-I battery unit: $R_B = 0.05\ \Omega$.
2) N-C battery unit: $R_B = 0.073\ \Omega$.
3) L-A unit: $R_B = 0.104\ \Omega$.
4) Short-circuit time constant $\tau_{\text{SC}} = 3.3$ ms (Table II in Ref. [5]).

The values of $(I_{\text{SCB}})_{\max}$ are determined by the IEEE Standards 946 and 1375 as follows.

1) IEEE Standard 946:

$$(I_{\text{SCB}})_{\max} = \frac{V_{\text{Br}}}{R_B} \quad (9)$$

with V_{Br} being the rated terminal voltage.
2) IEEE standard 1375:

$$(I_{\text{SCB}})_{\max} = \frac{V}{R_B} \left(1 - e^{-\frac{t}{\tau_{bs}}} \right) \quad (10)$$

with V being the terminal voltage before the short-circuit.

Fig. 4 shows $(I_{\text{SCB}})_{\max}$ for the three battery units determined based on the SOC, as well as the IEEE Standards 946 and 1375. It can be seen from Fig. 4 that the IEEE Standards 946 and 1375 yield $(I_{\text{SCB}})_{\max}$ with higher values than that determined based on SOC. The differences between values of $(I_{\text{SCB}})_{\max}$ (as determined by IEEE Standards 1375 and 946, as well as the SOC) are due to the fact that IEEE Standards 1375 and 946 use rated values of terminal and internal voltages of the battery unit. These differences in $(I_{\text{SCB}})_{\max}$ are observed for the LI-I, L-C, and L-A battery units.

B. Effects of Controller Actions on the Short-Circuit Current

Battery chargers are usually operated by constant voltage and/or constant current controllers. Constant voltage controllers are designed to operate the charger (ac–dc PEC) to maintain the battery terminal voltage at a constant value by adjusting the charging current. Constant current controllers are designed to operate the charger to maintain a constant charging current until the battery terminal voltage meets a desired value [23], [24]. Refs. [23] and [24] have several designs for charger controllers.

A constant voltage-controlled 3ϕ charger (thyristor or switched ac-dc PEC) produces an average dc voltage, V_{dc} (over the nth switching interval) on its dc side as [24]

$$V_{\text{dc}}(n) = \frac{3}{2} V_{Ps}. \left(k(n) \right)_{\text{CV}} \quad (11)$$

where $(k(n))_{\text{CV}}$ $(0 \leq (k(n))_{\text{CV}} \leq 1)$ is related to the actions of the constant voltage controller during n, and V_{Ps} is the rms value of the line voltage on the ac side of the 3ϕ charger. The value of $(k(n))_{\text{CV}}$ depends on the type of charger as follows.
1) For a thyristor-based charger, $(k(n))_{\text{CV}}$ is

$$(k(n))_{\text{CV}} = \cos(\alpha(n))$$

with $\alpha(n)$ being the firing angle during n.

2) For a transistor-based charger, $(k(n))_{\text{CV}}$ is

$$(k(n))_{\text{CV}} = m_a(n)$$

with $m_a(n)$ being the modulation index during n.

The output dc current during n, I_{dc}, can be stated as [23], [24]

$$I_{\text{dc}}(n) = \frac{2(k(n))_{\text{CV}}}{\pi}\left(|i_a(n)| + |i_b(n)| + |i_c(n)|\right) \quad (12)$$

where $i_a(n), i_b(n), i_c(n)$ are the 3ϕ currents on the ac side of the charger during n. The value of $(k(n))_{\text{CV}}$ during n is set by the constant voltage controller to achieve

$$V_{\text{dc}}(n) \xrightarrow{(k(n))_{\text{CV}}} V_{\text{dc}}^*(n) \quad (13)$$

where $V_{\text{dc}}^*(n)$ is the desired output dc voltage.

A constant current-controlled charger will maintain I_{dc} fixed as long as $V_{\text{dc}} = V_{\text{dc}}^*$. For a 3ϕ charger operated by a constant current controller, the output dc voltage during n is stated as [24]

$$V_{\text{dc}}(n) = \frac{3}{2}V_s.(1 - k1_{\text{CC}}\Delta V_{\text{dc}}(n)) \quad (14)$$

where $k1_{\text{CC}}$ is a parameter of the constant current controller, and $\Delta V_{\text{dc}}(n)$ is given as

$$\Delta V_{\text{dc}}(n) = V_{\text{dc}}^* - V_{\text{dc}}(n).$$

The dc current, during n, produced by a 3ϕ constant current-controlled charger can be expressed as [24]

$$I_{\text{dc}}(n) = (\beta_0 + \beta_1 \Delta V_{\text{dc}}(n))(|i_a(n)| + |i_b(n)| + |i_c(n)|) \quad (15)$$

with β_0, β_1 being parameters for the constant current controller.

A short-circuit on the dc bus results in a sudden reduction of V_{dc}, and thus $\Delta V_{\text{dc}}(n) \neq 0$. The sudden reduction in V_{dc} triggers a response from the charger controller to restore V_{dc} to its desired value V_{dc}^*. A constant voltage controller will increase $(k(n))_{\text{CV}}$ to restore V_{dc}, causing I_{dc} to increase [see (12)]. A similar action will be initiated by a constant current controller, which tends to achieve $\Delta V_{\text{dc}} \to 0$. This action causes I_{dc} to increase as in (15). Since the response of a battery unit is slower than the response of the charger controller, fast increases in I_{dc} can affect I_{SCB} (the short-circuit current contributed by a battery unit).

The actions of charger controller (constant voltage or constant current) to restore V_{dc} will slow the decay of SOC, as a high current is drawn from the battery unit (due to a short-circuit at the dc bus). This can be illustrated by [25]

$$V_{\text{dc}}(n) = V_{B0} - \frac{C.h_p(1 - \text{SOC}(n))}{\text{SOC}(n)}$$

$$- \left(\frac{h_p}{\text{SOC}(n)} + R_B\right)(I_{DS})_{\text{Rated}} \quad (16)$$

where V_{B0} is the battery internal potential, and h_p is the polarization coefficient. The effects of V_{dc} on the SOC for LI-I, N-C, and L-A battery units are demonstrated in Fig. 5. The curves in Fig. 5 are obtained using the following data [21], [22]:

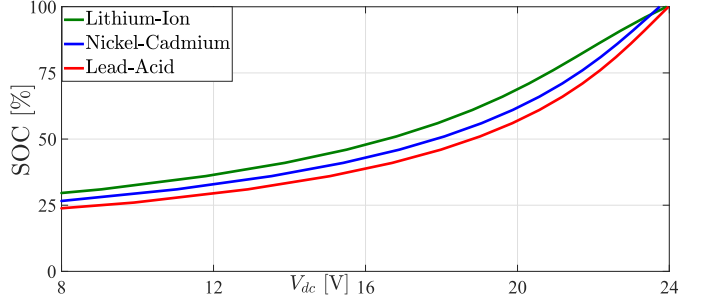1) Li-I: $V_{B0} = 25.59$ V, $h_p = 0.1484$, $(I_{DS})_{\text{Rated}} = 8$ A, $R_B = 0.050\ \Omega$.

Fig. 5. Effects of changing V_{dc} (produced by the charger) on the SOC for the tested lithium-ion, nickel–cadmium, and lead-acid battery units.

2) N-C: $V_{B0} = 25.70$ V, $h_p = 0.1406$, $(I_{DS})_{\text{Rated}} = 8$ A, $R_B = 0.073\ \Omega$.

3) L-A: $V_{B0} = 25.93$ V, $h_p = 0.1373$, $(I_{DS})_{\text{Rated}} = 8$ A, $R_B = 0.104\ \Omega$.

It can be observed from Fig. 5 that regulating the terminal voltage of a battery unit will prevent the fast decay of the SOC. This observation is applicable to the three tested battery units. The adjustment of the SOC will change the maximum short-circuit current that can be drawn from a battery unit. It should be noted that Fig. 5 does not provide any relationship between the SOC and battery open-circuit terminal voltage (VOC).

In order to demonstrate the effects of charger controller actions, two models for chargers were constructed. One model was for a 3ϕ, 0.25 kW, 60 Hz, thyristor-based charger, which had an ac-side line voltage of 20 V. Another model was for a 3ϕ, 0.25 kW, 60 Hz, insulated-gate bipolar transistor (IGBT)-based charger, which had an ac-side line voltage of 20 V [21], [22]. Each of the tested LI-I, N-C, and L-A battery units was separately fed by the two chargers. Constant voltage and constant current controllers were designed, and employed to operate the thyristor and IGBT chargers. For each charger feeding each battery unit, a short-circuit was created at the terminals of the battery unit. For each short-circuit, $(I_{\text{SCB}})_{\text{max}}$ was measured, and plotted as shown in Fig. 6.

It can be seen from Fig. 6 that both charger controllers managed to reduce $(I_{\text{SCB}})_{\text{max}}$ (relative to Fig. 4) for the three tested battery units. The reductions in $(I_{\text{SCB}})_{\text{max}}$ could also be observed for thyristor and IGBT chargers, when operated by constant voltage and constant current controllers. Observed reductions in $(I_{\text{SCB}})_{\text{max}}$ resulted from actions of the charger controller to adjust V_{dc} to its desired value during the short circuit at the dc bus. The adjustments in V_{dc} did allow the SOC to quickly change, thus limiting the discharge current during the short-circuit at the dc bus.

IV. TESTING BATTERY CONTRIBUTIONS TO FAULT CURRENTS IN GRID-CONNECTED BSSs

The testing of battery contributions to fault currents was conducted for a 1-MW grid-connected BSS. This BSS was modeled using e-TAP, and its controller parameters were selected using MATLAB/SIMULINK tools. The tested BSS was operated for frequency regulation, which required a frequency
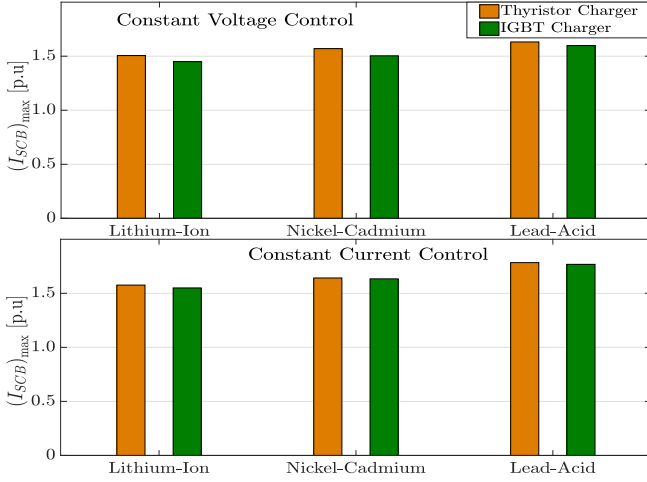
Fig. 6. Effects of charger controller actions on $(I_{SCB})_{\max}$ for the tested lithium-ion, nickel–cadmium, and lead-acid battery units. The base value of I_{SCB} is 8 A. $k_{CV} = 0.84$, $k1_{CC} = 0.63$, $\beta1 = 0.92$, $\beta2 = 0.24$.

Fig. 7. A single-line diagram for the test 1 MW grid-connected BSS. $\mathbf{i0} = [i_{a0}, i_{b0}, i_{c0}]$ and $\mathbf{i1} = [i_{a1}, i_{b1}, i_{c1}]$.

TABLE I
DATA FOR THE TEST 1 MW, 3ϕ, GRID-CONNECTED BSS

Parameter	Value
Rated DC Bus Voltage	960 V
Battery Type	Lead-Acid
Energy Capacity	240 kWh
Capacity	260 Ah
Maximum DoD	20%
Parallel Strings	30
R_B for Each String	6.26 Ω
Rated Current for Each String	34.5 A
Charger Type	Bi-Directional IGBT PEC
Charger Rated Current	770 A
Charger Pulsed Current	1600 A (over 1.5 ms)
Charger Controller	Constant Voltage: $k_{CV} = 0.78$
Frequency Droop Controller	$G_D = 0.3$, DB = [49.9, 50.1] Hz
Rated AC Bus Voltage	960 V
Grid-Tie Filter	$L = 6.0$ mH
Grid-Connection Transformer	1.2 MVA, 11/0.96 kV, 60 Hz, $\Delta - Y$

G_D: the droop constant; DB: the frequency dead-band; DoD: depth of discharge.

TABLE II
LOAD FLOW RESULTS FOR THE CHARGING OPERATION OF THE
GRID-CONNECTED BSS

Quantity	Magnitude	Angle
i_{a0}	46.1 A	-2.86°
i_{b0}	46.1 A	-122.86°
i_{c0}	46.1 A	117.14°
i_{a1}	595.8 A	-3.03°
i_{b1}	595.8 A	-123.03°
i_{c1}	595.8 A	116.97°
I_{dc}	436.4 A	
I_B	436.4 A	
v_a	0.95 kV	-0.03°
v_b	0.95 kV	-120.03°
v_c	0.95 kV	119.97°
V_{dc}	0.96 kV	

droop controller as a second controller. The data for the tested grid-connected BSS is listed in Table I. Fig. 7 shows a single-line diagram for the test grid-connected BSS.

The e-TAP model for the test grid-connected BSS was tested for several fault events. The following fault events are presented and discussed in this article.

1) Charging and discharging operations of the BSS.
2) Short-circuit on the dc bus during the charging operation.
3) Line-to-ground fault during the discharging operation.
4) Line-to-line fault during the charging operation.

A. Charging and Discharging Operations of the BSS

This test aimed to investigate the normal operating modes of the test grid-connected BSS. The charging and discharging operations were tested through the load flow analysis. The charging operation was conducted with SOC set as SOC = 80%. It should be noted that SOC = 80% was selected as it represented the lowest acceptable SOC for the used L-A battery units. As a
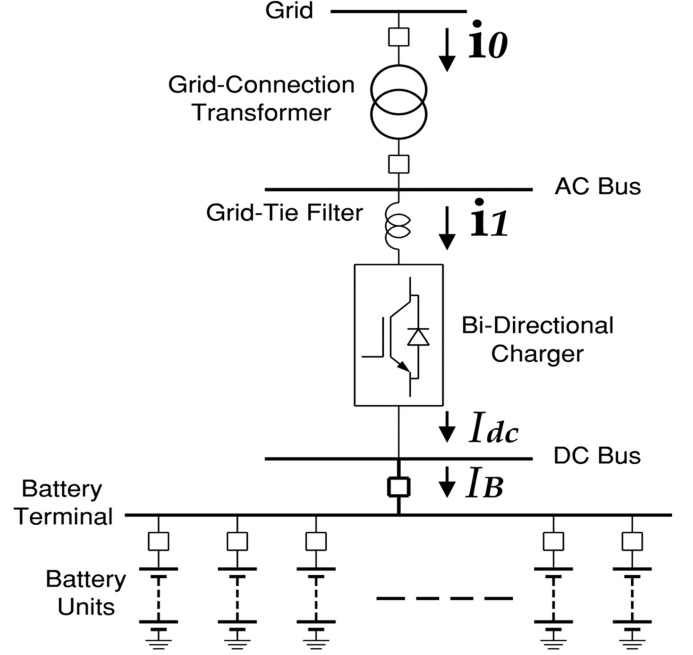
result, SOC = 80% provided the maximum charging current for the tested grid-connected BSS. The 3ϕ currents $\mathbf{i0}$, $\mathbf{i1}$, dc currents I_{dc}, I_B, ac bus voltage, and dc bus voltage were collected for the charging operation as listed in Table II. The discharging operation was initialized for SOC = 96%, to ensure high discharging current. The grid-connected BSS injected power into the grid as follows:

$$P = 992 \; [\text{kW}] \text{ and } Q = 86 \; [\text{kVAR}]. \tag{17}$$

Table III lists the 3ϕ currents $\mathbf{i0}$, $\mathbf{i1}$, dc currents I_{dc}, I_B, ac bus voltage, and dc bus voltage obtained from the load flow analysis for the discharging operation of the grid-connected BSS. It should be noted that the currents in Table III were taken with the convention that currents flowing from the grid had positive sign.

The results in Tables II and III demonstrated stable charging and discharging operations of the tested grid-connected BSS.

TABLE III

LOAD FLOW RESULTS FOR THE DISCHARGING OPERATION OF THE GRID-CONNECTED BSS

Quantity	Magnitude	Angle
i_{a0}	-52.9 A	-5.15°
i_{b0}	-52.9 A	-125.15°
i_{c0}	-52.9 A	114.85°
i_{a1}	-683.7 A	-4.62°
i_{b1}	-683.7 A	-124.62°
i_{c1}	-683.7 A	115.38°
I_{dc}	-500.8 A	
I_B	-500.8 A	
v_a	0.95 kV	-0.02°
v_b	0.95 kV	-120.02°
v_c	0.95 kV	119.98°
V_{dc}	0.96 kV	

TABLE IV

RESULTS FOR THE SHORT-CIRCUIT AT THE DC BUS DURING CHARGING OPERATION WITH THE CONSTANT VOLTAGE CONTROLLER

Quantity	Magnitude	Angle
i_{a0}	16.73 A	-30.1°
i_{b0}	16.73 A	-150.1°
i_{c0}	16.73 A	89.9°
i_{a1}	216.09 A	-32.2°
i_{b1}	216.09 A	-152.3°
i_{c1}	216.09 A	87.8°
I_{dc}	198.27 A	
I_B	-282.94 A	
v_a	0.91 kV	-3.8°
v_b	0.91 kV	-123.8°
v_c	0.91 kV	116.2°
V_{dc}	0.92 kV	

TABLE V

RESULTS FOR THE SHORT-CIRCUIT AT THE DC BUS DURING CHARGING OPERATION WITHOUT THE CONSTANT VOLTAGE CONTROLLER

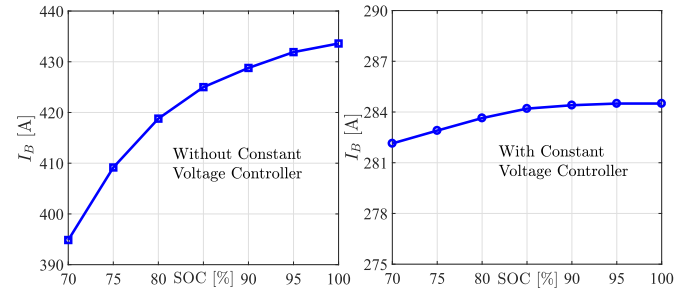| Quantity	Magnitude	Angle
i_{a0}	4.78 A	-11.9°
i_{b0}	4.78 A	-131.8°
i_{c0}	4.78 A	108.1°
i_{a1}	61.74 A	-13.2°
i_{b1}	61.74 A	-133.1°
i_{c1}	61.74 A	106.8°
I_{dc}	45.22 A	
I_B	-418.79 A	
v_a	0.92 kV	-0.04°
v_b	0.92 kV	-120.04°
v_c	0.92 kV	119.96°
V_{dc}	0.83 kV	

Fig. 8. Contribution of the battery units to the short-circuit current, I_B, at the dc bus for different values of SOC, with and without the actions of the constant voltage controller.

These results also showed that during steady-state conditions, I_{dc} and I_B had identical values. This feature was a result from the absence of any loads connected to the dc bus, and confirmed the power flow from and to the battery units. Finally, the data obtained from this test provided a base case for the steady-state operation of the grid-connected BSS.

B. Short-Circuit on the DC Bus During the Charging Operation

The objective of this test was to examine the contribution of the battery units to a short-circuit at the dc bus during the charging operation. The short-circuit was created through a resistance of $R_F = 2$ Ω, with SOC $= 80\%$. The short-circuit analysis tool of e-TAP was used to determine the currents through the grid-connected BSS. The 3ϕ currents **i**0, **i**1, dc currents I_{dc}, I_B, ac bus voltage, and dc bus voltage were collected for the short-circuit at the dc bus, and listed in Table IV. It should be noted that I_B had a negative sign to indicate its direction was out of the battery units. For purposes of demonstrating the effects of the charger controller, the short-circuit at the dc bus was created with constant voltage controller disabled. Table V lists the 3ϕ currents **i**0, **i**1, dc currents I_{dc}, I_B, ac bus voltage, and dc bus voltage for the short-circuit at the dc bus.

The results of this test demonstrated the effects of the charger controller on battery contributions to the short-circuit current. The data in Tables IV and V showed that actions of the constant voltage controller supported V_{dc} by increasing I_{dc}. These actions

resulted in limiting I_B flowing to the short-circuit branch. The changes in I_{dc}, I_B, and V_{dc} could be seen from the values of these quantities in Tables IV and V.

In order to demonstrate the effects of charger controller and SOC on I_B, the short-circuit at the dc bus was created for several values of SOC with and without the actions of the constant voltage controller. Fig. 8 shows I_B due to the short-circuit at the dc bus, for several values of SOC with and without the charger controller. The results in Fig. 8 showed the effects of the charger controller and SOC on the contribution of battery units to the short-circuit current. Actions of the constant voltage controller regulated V_{dc} (prevented its fast decline) and limited I_B (prevented its transient increase) during the short-circuit at the dc bus.

C. Line-to-Ground Fault During the Discharging Operation

This test aimed to examine the contribution of the battery units to a line-to-ground fault on the ac bus during the discharging operation. The phase B-to-ground fault was created through a resistance of $R_F = 1$ Ω, with SOC $= 100\%$. The short circuit analysis tool of e-TAP was used to determine the currents through the grid-connected BSS. The 3ϕ currents **i**0, **i**1, dc currents I_{dc}, I_B, ac bus voltage, and dc bus voltage were collected for the fault at the ac bus, and listed in Table VI.

The data in Table VI shows that the phase B-to-ground fault on the ac bus caused an imbalance in the currents flowing from the BSS to the grid, as well as the currents on the grid side. The ground fault also resulted in a significant increase in i_{b1}

TABLE VI
RESULTS FOR THE PHASE B-TO-GROUND FAULT AT THE
AC BUS DURING THE DISCHARGING OPERATION

Quantity	Magnitude	Angle
i_{a0}	475.78 A	-54.1°
i_{b0}	521.87 A	125.4°
i_{c0}	46.28 A	-60°
i_{a1}	601.38 A	-30°
i_{b1}	2376.78 A	-52.9°
i_{c1}	601.38 A	90°
I_{dc}	466.87 A	
I_B	466.87 A	
v_a	0.90 kV	-1.9°
v_b	0.80 kV	-63.2°
v_c	0.92 kV	122.2°
V_{dc}	0.94 kV	

TABLE VII
RESULTS FOR THE PHASE A-TO-PHASE C FAULT IN THE
CHARGER PEC DURING THE CHARGING OPERATION

Quantity	Magnitude	Angle
i_{a0}	49.6 A	-47.6°
i_{b0}	24.1 A	-115.9°
i_{c0}	49.6 A	90.9°
i_{a1}	640.8 A	-52.4°
i_{b1}	310.6 A	-118.9°
i_{c1}	641.1 A	94.8°
I_{dc}	-328.2 A	
I_B	-388.2 A	
v_a	0.92 kV	-1.9°
v_b	0.94 kV	-122.2°
v_c	0.91 kV	174.9°
V_{dc}	0.92 kV	

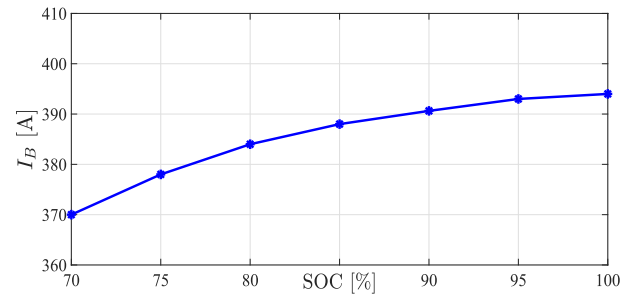Fig. 9.   Effects of SOC on I_B triggered by the phase B-to-ground at the ac bus.

Fig. 10.   Effects of SOC on I_B triggered by a line-to-line fault (phase A-to-phase C fault) in the charger PEC.

TABLE VIII
BATTERY CURRENT AND TERMINAL VOLTAGE DURING FAULTS IN DIFFERENT
LOCATIONS IN A GRID-CONNECTED BSS

Fault	With Controller	Without Controller	IEEE Standards
Short-Circuit at DC Bus	I_B = 286.5 A V_{dc} = 0.93 kV	I_B = 433.6 A V_{dc} = 0.78 kV	I_B = 4064.9 A V_{dc} = 0.96 kV
3ϕ Fault at AC Bus	I_B = 329.7 A V_{dc} = 0.94 kV	I_B = 731.3 A V_{dc} = 0.72 kV	I_B = 7700 A V_{dc} = 0.96 kV
Line-to-Ground at AC Bus	I_B = 466.8 A V_{dc} = 0.94 kV	I_B = 882.4 A V_{dc} = 0.77 kV	I_B = 7700 A V_{dc} = 0.96 kV
Line-to-Line at AC Bus	I_B = 394.6 A V_{dc} = 0.93 kV	I_B = 782.2 A V_{dc} = 0.80 kV	I_B = 7700 A V_{dc} = 0.96 kV

due to the increase in I_B and the reversal of i_{b0}. Moreover, the line-to-ground fault on the ac bus caused changes in the ac voltages and V_{dc}. The phase B-to-ground at the ac bus was tested for several values of SOC to demonstrate the effects of SOC on I_B. Fig. 9 shows I_B, triggered by the fault at the ac bus, for several values of SOC.

The results in Fig. 9 showed that the SOC affected the contribution of battery units to the line-to-ground fault at the ac bus. The effects of SOC on I_B triggered by the phase B-to-ground fault were in agreement with the results in Fig. 8 (the short-circuit at the dc bus).

D. Line-to-Line Fault During the Charging Operation

The objective of this test was to examine the contribution of battery units to a line-to-line fault in the charger PEC during the charging operation. The phase A-to-phase C fault was created through a resistance of $R_F = 3\ \Omega$, with SOC = 88%, and with the constant voltage controller. Table VII lists the 3ϕ currents i0, i1, dc currents I_{dc}, I_B, ac bus voltage, and dc bus voltage for the tested asymmetrical fault in the charger PEC.

The data in Table VII shows that the phase A-to-phase C fault in the charger PEC resulted in unbalanced currents flowing from the grid, and voltages on ac bus. The line-to-line fault caused significant increases in i_{a1} and i_{c1} due to the fault. In addition, I_B and I_{dc} reversed their direction as battery units contributed to the fault current. Finally, the phase A-to-phase C fault in the charger PEC changed the ac voltages and V_{dc}. Similar to the other tested faults, this line-to-line fault was tested for several values of SOC, as shown in Fig. 10.

Fig. 10 demonstrated the effects of SOC on the contribution of battery units to the line-to-line fault in the charger PEC. The results in Fig. 10 were consistent with results obtained from other faults, where SOC had direct impacts on I_B.

The tested cases have demonstrated the effects of the SOC and actions of the charger controller on the contributions of battery units to faults in grid-connected BSSs. In all tested cases, low SOC values have resulted in lower currents drawn from battery units due to fault events. Furthermore, actions of charger controller have been found able to limit the reductions in dc voltage at battery terminals. These controller actions have resulted in limiting the contributions of battery units to fault currents. These effects of the SOC and charger controller have been observed for faults in different locations of the grid-connected BSS. Finally, the effects of the SOC and charger controller on battery contributions to fault currents have been observed during the charging and discharging operation. Table VIII provides a summary of I_B and V_{dc} for different fault events at different

locations of a grid-connected BSS. These values are determined at SOC = 100%, with and without controller actions (constant voltage), and using IEEE Standard 1375 and IEEE Standard 946.

The data in Table VIII shows the effects of the charger controller on battery currents and terminal voltage due to faults in different locations of a grid-connected BSS. The data in Table VIII together with Figs. 9 and 10 confirm the effects of the SOC and charger controller on I_B and V_{dc} for fault conditions. Observed effects of the SOC and charger controller on I_B and V_{dc} can be used for developing accurate and reliable detection of faults in grid-connected BSSs.

V. Conclusion

This article has presented the factors that affect battery contributions to fault currents in grid-connected BSSs. The typical determination of battery contributions to fault currents is based on IEEE Standards 1375 and 946, which use the rated battery terminal voltage and internal resistance. These standards are widely used to select and size protective devices for battery units used in stationary BSSs (see Fig. 2). Grid-connected BSSs do not have loads connected to the dc bus, and thus battery currents only flow through the charger PEC. Battery currents are directly related to the SOC and actions of the charger controller. Effects of the SOC and charger controller on the currents drawn from battery units due to faults have been investigated for the charging and discharging operations. Investigation results have shown that the currents drawn from battery units, due to faults, are directly related to the SOC and actions of charger controller. Observed effects can be critical for developing fault detection methods to improve the protection and operation of grid-connected BSSs.

References

[1] S. A. Saleh et al., "Factors affecting battery unit contributions to fault currents in grid-connected battery storage systems," in *Proc. 56th IEEE IAS Annu. Meeting Conf.*, Vancouver, BC, Canada, 2021, pp. 1–8.

[2] *IEEE Application Guide for IEEE Standard for Interconnecting Distributed Resources With Electric Power Systems*, IEEE Std. 1547.2-2008, 2008, pp. 1–217.

[3] *IEEE Recommended Practice for the Design of DC Power Systems for Stationary Applications*, IEEE Std. 946–2020, 2020, pp. 1–74.

[4] *IEEE Recommended Practice for Sizing Lead-Acid Batteries for Stand Alone Photovoltaic (PV) Systems*, IEEE Std.1013-2007, 2007, pp. 1–50.

[5] *IEEE Guide for the Protection of Stationary Battery Systems*, IEEE Std. 1375–1998, 1998, pp. 1–59, doi: 10.1109/IEEESTD.1998.87900.

[6] *IEEE Recommended Practice for Industrial and Commercial Power Systems Analysis*, IEEE Std. 399–1997, 1997, pp. 1–488.

[7] S. A. Saleh, E. Ozkop, C. Mardegan, and M. Valdes, "Bus differential protection for buses interconnecting battery storage systems," in *Proc. 57th IEEE IAS Ind. Commercial Power Syst. Tech. Conf.*, Las Vegas, NV, USA, 2021, pp. 1–8.

[8] G. Wang et al., "A review of power electronics for grid connection of utility-scale battery energy storage systems," *IEEE Trans. Sustain. Energy*, vol. 7, no. 4, pp. 1778–1790, Oct. 2016.

[9] M. Farhadi and O. Mohammed, "Energy storage technologies for high-power applications," *IEEE Trans. Ind. Appl.*, vol. 52, no. 3, pp. 1953–1961, May/Jun. 2016.

[10] M. A. Haj-ahmed and M. S. Illindala, "Investigation of protection schemes for flexible distribution of energy and storage resources in an industrial microgrid," *IEEE Trans. Ind. Appl.*, vol. 51, no. 3, pp. 2071–2080, May/Jun. 2015.

[11] P. Rakhra, P. J. Norman, S. D. A. Fletcher, S. J. Galloway, and G. M. Burt, "Evaluation of the impact of high-bandwidth energy-storage systems on DC protection," *IEEE Trans. Power Del.*, vol. 31, no. 2, pp. 586–595, Apr. 2016.

[12] S. A. Saleh, C. Richard, X. F. St-Onge, J. Meng, and E. Castillo-Guerra, "Comparing the performance of protection coordination and digital modular protection for grid-connected battery storage systems," *IEEE Trans. Ind. Appl.*, vol. 55, no. 3, pp. 2440–2454, May/Jun. 2019.

[13] S. A. Saleh, R. McSheffery, and R. Meng, "Testing the performance of the digital modular protection for grid-connected battery storage systems," *IEEE Trans. Ind. Appl.*, vol. 54, no. 3, pp. 2059–2070, May/Jun. 2018.

[14] A. C. Gaunce et al., "DC arc flash: Testing and modeling incidents in a 125-V substation battery backup system," *IEEE Trans. Ind. Appl.*, vol. 56, no. 3, pp. 2138–2147, May/Jun. 2020.

[15] R. Hedding and P. Hayes, "Protection of battery energy storage system," in *Proc. 64th IEEE Annu. Conf. Protective Relay Engineers*, College Station, TX, USA, 2011, pp. 155–159.

[16] L. Tao, G. Chunlin, Y. Jingjing, W. Jianing, Z. Chenliang, and M. Huiyuan, "Analysis on DC side protection strategy for grounded power battery energy storage system," in *Proc. IEEE IAS Ind. Commercial Power Syst. Asia Tech. Conf.*, Weihai, China, 2020, pp. 1006–1011.

[17] S. A. Saleh, A. S. Aljankawey, B. Alsayid, and M. S. Abu-Khaizaran, "Influences of power electronic converters on voltage-current behaviors during faults in DGUs-Part II: Photovoltaic systems," *IEEE Trans. Ind. Appl.*, vol. 51, no. 4, pp. 2832–2845, Jul./Aug. 2015.

[18] W. Hartmann, R. Fleck, R. Graba, and M. Hergt, "Characterization of commercial IGBT modules for pulsed power applications," in *Proc. 13th IEEE Pulsed Power Conf.*, San Francisco, CA, USA, 2013, pp. 1–4.

[19] *IEEE Recommended Practice for Conducting Short-Circuit Studies and Analysis of Industrial and Commercial Power Systems*, IEEE Std. 3002. 3–2018, 2018, pp. 1–184.

[20] M. Coleman, C. K. Lee, C. Zhu, and W. G. Hurley, "State-of-charge determination from EMF voltage estimation: Using impedance, terminal voltage, and current for lead-acid and lithium-ion batteries," *IEEE Trans. Ind. Electron.*, vol. 54, no. 5, pp. 2550–2557, Oct. 2007.

[21] *Power System Toolbox User Guide*. Natick, MA, USA: Math Works, 2017.

[22] "e-TAP 19.01: Short circuit analysis toolbox," e-TAP, Irvine, CA, USA, 2019.

[23] D. Sha, G. Xu, and Y. Xu, "Utility direct interfaced charger/discharger employing unified voltage balance control for cascaded H-bridge units and decentralized control for CF-DAB modules," *IEEE Trans. Ind. Electron.*, vol. 64, no. 10, pp. 7831–7841, Oct. 2017.

[24] R. Metidji, B. Metidji, and B. Mendil, "Design and implementation of a unity power factor fuzzy battery charger using an ultrasparse matrix rectifier," *IEEE Trans. Power Electron.*, vol. 28, no. 5, pp. 2269–2276, May 2013.

[25] L. Y. Wang, M. P. Polis, G. G. Yin, W. Chen, Y. Fu, and C. C. Mi, "Battery cell identification and SOC estimation using string terminal voltage measurements," *IEEE Trans. Veh. Technol.*, vol. 61, no. 7, pp. 2925–2935, Sep. 2012.

Saleh A. Saleh (Senior Member, IEEE) received the B.Sc. degree in electrical engineering from Bir Ziet University, West Bank, Palestine, in 1996, and the M.Eng. and Ph.D. degrees in electrical engineering from the Memorial University of Newfoundland, St. John's, NL, Canada, in 2003 and 2007, respectively, with a scholarship from the Natural Sciences and Engineering Research Council of Canada (NSERC).

He was with Palestinian Technical College, West Bank, Palestine, as an Instructor and a Program Coordinator until 2001. From 2007 to 2011, he was a Faculty and a Researcher with Marine Institute, Memorial University of Newfoundland. He is currently a Professor with the Department of Electrical and Computer Engineering, University of New Brunswick, Fredericton, NB, Canada. His research interests include power system operation, control, and protection, digital protection of energy conversion systems, power electronic converter design, analysis, operation, and control, renewable energy systems, motor drives, and digital signal processing applications in power systems, power electronic converters, and motor drives.

Dr. Saleh's research works are supported by the Natural Sciences and Engineering Research Council and New Brunswick Innovation Foundation. He is a registered Professional Engineer in the Provinces of Newfoundland and Labrador and New Brunswick, Canada. He is a recipient of the 2015 Harrison McCain Young Scholars Award and the 2020 University of New Brunswick Merit Award.

Emre Ozkop (Senior Member, IEEE) received the B.Sc.E. degree in electrical and electronics engineering from Gazi University, Ankara, Turkey, in 2003, and the M.Sc.E. and Ph.D. degrees in electrical engineering from Karadeniz Technical University (KTU), Trabzon, Turkey, in 2006 and 2012, respectively.

He is currently an Associate Professor with the Department of Electrical and Electronics Engineering, KTU. He was a Visiting Scholar with the University of New Brunswick, Fredericton, NB, Canada, in 2015 and 2017. His research interests include power electronics, intelligent control systems, power systems protection, control, and grounding, renewable energy systems operation, control, and protection, and smart grid implementation and deployment.

Mohammed Haj-Ahmed (Member, IEEE) received the B.Sc. degree from the University of Jordan, Amman, Jordan, in 2006, and the M.Sc. and Ph.D. degrees from Ohio State University, Columbus, OH, USA, in 2011 and 2015, respectively, all in electrical engineering.

Since 2015, he has been with the Department of Electrical and Computer Engineering, University of Jordan, where he is currently an Associate Professor. His research interests include power systems control and protection, power system communication, microgrid protection, renewable energy systems, and control systems.

Dr. Haj-Ahmed is registered with Jordan Engineers Association.

Marcelo E. Valdes (Fellow, IEEE) received the B.S. degree in electrical engineering from Cornell University, Ithaca, NY, USA, in 1977.
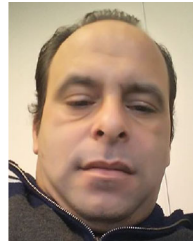
He was with GE for 41 years in the field engineering, sales, product management, marketing, and application engineering. He was with the Electrical Products Division, ABB, Cary, NC, USA, in 2018. He is a registered Professional Engineer. He has authored or coauthored more than 35 technical papers for IEEE and other engineering forums. He holds 28 patents in the field electrical distribution and control.

Valdes was the Chair of various IEEE PES and IAS chapters in Northern California, and the Chair of the 2014 IEEE Electrical Safety Workshop (IEEE-ESW). He is the Chair of the IEEE 1683-2014 working group for the IEEE P1683 Guide for Specification and Selection of Low Voltage Motor Control Centers with Enhanced Safety Features. He is active in various IEEE working groups, mostly in electrical safety and power system protection. He has participated in CSA Z462, the Canadian Electrical Safety Standard, NFPA 70, the NEC, and NFPA70B NFPA's Electrical Maintenance Standard. He has received recognition for his contributions from the Pulp & Paper Industry Committee and IEEE Electrical Safety Committee; and has received the 2015 Pulp & Paper Industry Committee Meritorious Engineering Award, the Excellence in Prevention Through Design Technical Award, and the IEEE IAS Applications Magazine First Prize Article Award in 2014.

Zaid G. Sanchez (Member, IEEE) received the B.Sc. degree from the Universidad Central de las Villas, Santa Clara, Cuba, in 2002, and the M.Sc. and Ph.D. degrees from the Universidad Central de las Villas, Cuba, in 2004 and 2011, respectively, all in electrical engineering.

Since 2012, he has been an Assistant Professor with the Center for Energy and Environment Studies (CEEMA), University of Cienfuegos, Cienfuegos, Cuba, where he is currently a Professor and the Head. From 2018 to 2019, he was a Visiting Scholar with Emera & NB Power Research Center for Smart Grid Technologies, University of New Brunswick, Fredericton, NB, Canada. His research interests include power system modeling, stability analysis, planning, and protection. His research works also involve integrating and operating renewable energy sources, as well as developing and planning smart grid functions.

Ahmet Yuksel (Student Member, IEEE) received the B.Sc. and M.Sc. degrees in electrical and electronics engineering from Karadeniz Technical University (KTU), Trabzon, Turkey, in 2015 and 2018, respectively. He is currently working toward the Ph.D. degree in electrical engineering with Gazi University, Ankara, Turkey.

He is a Researcher with the Energy Institute of Scientific and Technological Research Council of Turkey (TUBITAK), Marmara Research Center (MRC), Ankara, Turkey. His research interests include power electronic converter design, analysis, operation, control, and renewable energy systems.

Claudio S. Mardegan (Senior Member, IEEE) received the Electrical Engineering degree in Electrical Power System Engineer from the Federal University of Itajuba (UNIFEI), Itajuba, Brazil, in 1980.

He is a Director of EngePower, Osasco, Brazil. He is a Consulting Engineer for Brazilian and multinational companies and an Instructor of several courses in protection engineering. He is the Author of the Proteço e Seletividadeem Sistemas Eletricos Industriais (Protection and Coordination in Electrical Power Systems; Attitude Editorial, 2012). He is the Co-Author of the Guide for Low Voltage and Medium Voltage (Brazilian Standards NBR-5410 and NBR-14039). He has authored many papers in the areas of power system analysis and protection systems. He has extensive experience in design, assembling, commissioning, maintenance, consulting, and analysis of power systems and protection systems.

Mardegan has participated in the Generator Grounding, Forensics, DC, and 3004-Series Working Groups in IEEE Industrial Applications Society.